

## Article

# Experimental Study on the Effect of Hydrogen Addition on the Laminar Burning Velocity of Methane/Ammonia–Air Flames

Ahmed Yasiry<sup>1,2</sup>, Jinhua Wang<sup>1,\*</sup> , Longkai Zhang<sup>1</sup>, Hongchao Dai<sup>1</sup>, Ahmed A. A. Abdulraheem<sup>3</sup>, Haroun A. K. Shahad<sup>3</sup> and Zuohua Huang<sup>1</sup>

<sup>1</sup> State Key Laboratory of Multiphase Flow in Power Engineering, Xi'an Jiaotong University, Xi'an 710049, China

<sup>2</sup> Automotive Engineering Department, College of Engineering-Musaib, University of Babylon, Babil 51002, Iraq

<sup>3</sup> Mechanical Engineering Department, College of Engineering, University of Babylon, Babil 51002, Iraq

\* Correspondence: [jinhuaawang@mail.xjtu.edu.cn](mailto:jinhuaawang@mail.xjtu.edu.cn)

**Abstract:** Variations in methane–ammonia blends with hydrogen enrichment can modify premixed flame behavior and play a crucial role in achieving ultra-low carbon emissions and sustainable energy consumption. Current combustion units may co-fire ammonia/methane/hydrogen, necessitating further investigation into flame characteristics to understand the behavior of multi-component fuels. This research aims to explore the potential of replacing natural gas with ammonia while making only minor adjustments to equipment and processes. The laminar burning velocity (LBV) of binary blends, such as ammonia–methane, ammonia–hydrogen, and hydrogen–methane–air mixtures, was investigated at an equivalence ratio of 0.8–1.2, within a constant volume combustion chamber at a pressure of 0.1 MPa and temperature of 298 K. Additionally, tertiary fuels were examined with varying hydrogen blending ratios ranging from 0% to 40%. The results show that the laminar burning velocity (LBV) increases as the hydrogen fraction increases for all mixtures, while methane increases the LBV during blending with ammonia. Hydrogen–ammonia blends are the most effective mixture for increasing LBV non-linearly. Enhancement parameters demonstrate the effect of ternary fuel, which behaves similarly to equivalent methane in terms of adiabatic flame temperature and LBV achieved at 40% hydrogen. Experimental data for neat and binary mixtures were validated by different kinetics models, which also showed good consistency. The ternary fuel mixtures were also validated with these models. The Li model may qualitatively predict well for ammonia-dominated fuel. The Shrestha model may overestimate results on the rich side due to the incomplete  $N_2H_2$  sub-mechanism, while lean and stoichiometric conditions have better predictions. The Okafor model is always overestimated.

**Keywords:** laminar burning velocity; ternary fuel blending; ammonia; methane; hydrogen



**Citation:** Yasiry, A.; Wang, J.; Zhang, L.; Dai, H.; Abdulraheem, A.A.A.; Shahad, H.A.K.; Huang, Z. Experimental Study on the Effect of Hydrogen Addition on the Laminar Burning Velocity of Methane/Ammonia–Air Flames. *Appl. Sci.* **2023**, *13*, 5853. <https://doi.org/10.3390/app13105853>

Academic Editor: Maria Grazia De Giorgi

Received: 13 April 2023

Revised: 27 April 2023

Accepted: 28 April 2023

Published: 9 May 2023



**Copyright:** © 2023 by the authors. Licensee MDPI, Basel, Switzerland. This article is an open access article distributed under the terms and conditions of the Creative Commons Attribution (CC BY) license (<https://creativecommons.org/licenses/by/4.0/>).

## 1. Introduction

There has been worldwide interest in finding solutions to the problems of fossil fuel shortage, air pollution, and climate change. Moreover, of concern is the kinetics of reactions, which can involve hundreds of reactants and form an enormous number of intermediate species. For these reasons, researchers have been looking into and implementing power and energy systems that operate on renewable, low-, or no-carbon fuels. The key outcomes of this application were in optimizing the engine conditions and the combustion characteristics, increasing energy efficiency, and pursuing a sustainable system and possibilities of alternate fuel for the combustion process [1].

Hydrogen and ammonia fuels are proposed as energy carriers to store and transport intermittent renewable energy sources, such as solar and wind, over long distances. They are also considered popular carbon-free fuels. The blending of hydrocarbons with hydrogen

or ammonia fuels has garnered tremendous attention from researchers in overcoming these challenges, given their popularity as carbon-free fuels. However, the diversity in the laminar burning velocity (LBV) is quite interesting. Hydrogen exhibits the highest LBV with vast flammability limits and low minimum ignition energy. In contrast, ammonia has not traditionally been considered as a fuel due to its lower combustion intensities and narrower flammability limits [2]. It has one of the lowest LBVs, approximately five times lower than that of methane [3], resulting in low burning efficiency in engines and high fuel NO<sub>x</sub> production, which contributes to significant environmental problems [4]. Moreover, ammonia exhibits lower adiabatic flame temperatures, high minimum ignition energy, and contains a nitrogen atom in its molecule. These can lead to a low heat release rate, poor flame stabilization, low combustion efficiency, and high fuel NO emissions [5]. However, ammonia is not only a suitable hydrogen carrier made up of 17.8% by weight of hydrogen, but it also offers higher hydrogen density (121 kg-H<sub>2</sub>/m<sup>3</sup>) compared to liquid hydrogen (70.8 kg-H<sub>2</sub>/m<sup>3</sup>), which makes it a more feasible alternative [6].

Table 1 demonstrates that hydrogen requires a very low temperature to liquefy compared with ammonia. This means that ammonia can be easily stored after liquefaction at room temperature and a pressure of 8.5 bar or cooled to −33.4 °C at ambient pressure. Hydrogen needs to be liquefied at room temperature and a pressure of 350–700 bar or at −252.9 °C as a liquid at ambient pressure [7]. It can be noticed that the storage of ammonia is much cheaper than hydrogen storage. Furthermore, the heat of combustion and LBV for ammonia compared with methane are 20% and 40%, respectively. Ammonia has the narrowest flammability range, the highest minimum autoignition temperature, and the lowest flame temperature. Moreover, the radiation heat transfer from the ammonia flame is lower than that of a hydrocarbon flame due to the lack of CO<sub>2</sub> in the product of ammonia combustion. However, the NO<sub>x</sub> emission remains a significant challenge. Moreover, the production, storage, and transportation of ammonia have already been well established as is the infrastructure for the distribution. In other words, compared with hydrogen, ammonia has lower storage pressure and volume by about 10 and 47 times, respectively. These are significant features in storage and transportation cost reduction [1]. Because of these advantages, ammonia represents a potentially valuable CO<sub>2</sub>-free fuel in fuel cells [8,9], gas turbines [10,11], boilers, or internal-combustion engines [12,13].

**Table 1.** Fundamental combustion characteristics and thermal properties of ammonia, hydrogen, and methane fuels [1].

Property/Fuel	NH <sub>3</sub>	H <sub>2</sub>	CH <sub>4</sub>
Boiling temperature at 0.1 MPa (°C)	−33.4	−252.9	−161
Lower heating value (MJ/kg)	18.6	120	50.0
Flammability limit ( $\phi$ )	0.63–1.40	0.10–7.1	0.50–1.7
Adiabatic flame temperature (K)	1800	2110	1950
Laminar burning velocity (m/s)	0.07	2.91	0.37
Auto ignition temperature (°C)	650	520	630

Laminar burning velocity ( $S_l$ ) is a physicochemical parameter that defines the movement of the reactant mixture to the reaction zone, encompassing mixing and reaction processes. It represents the fundamental aspects of combustion, including diffusion, exothermicity, and reactivity of fuel mixtures [14]. Accurate estimation of LBV data is crucial for understanding a wide range of flames and flame stabilization. Furthermore, it describes laminar and turbulent premixed characteristics within the laminar flamelet regime. LBV also plays a fundamental role in validating the chemical kinetics of the fuel and its combustion characteristics, such as flame stability, heat release rate, and diffusion probability. Therefore, it is a significant factor in calculating fuel performance and emissions [15–17].

Furthermore, according to the Gibbs free energy for the combustion product, the overall reaction for ammonia is  $4\text{NH}_3 + 3\text{O}_2 \rightarrow 2\text{N}_2 + 6\text{H}_2\text{O}$ , which indicates that there

are no final products of  $\text{NO}_x$ . When comparing the formation of NO in methane and ammonia, it is observed that NO produced from  $\text{NH}_3$ /air flames is lower than that from  $\text{CH}_4$ /air flames under stoichiometric conditions. This trend continues for lean conditions with increased NO production. However, for the rich side of stoichiometry, increasing the equivalence ratio leads to a more rapid decrease in NO generated from  $\text{NH}_3$ /air flames compared to  $\text{CH}_4$ /air flames [18]. In a few words, the mole fraction of NO produced by ammonia flames increases with an increase in the equivalence ratio ( $\phi$ ) and peaks at 0.9. However, beyond this point, there is a rapid decrease in the NO mole fraction on the rich side. When the equivalence ratio exceeds 1.3, NO production becomes almost negligible, typically around 10–100 parts per million (ppm). Rich side combustion is considered one of the effective methods for reducing  $\text{NO}_x$  emissions. However, it is important to note that this approach can lead to a sharp decrease in combustion efficiency due to the rapid increase in unburned  $\text{NH}_3$ . Another unwelcome product in the rich side combustion of ammonia is  $\text{N}_2\text{O}$ , which has a global warming potential 300 times higher than  $\text{CO}_2$  [1]. Given these observations, conducting slightly rich ammonia combustion would be preferable to achieve higher flame speed while minimizing the formation of  $\text{NO}_x$ .

#### *Ammonia Flame Enhancement by Fuel Blending*

Several researchers have successfully investigated neat ammonia as a promising fuel. This research has covered various aspects, including flame propagation speed, chemical kinetics, and its application in internal combustion engines and gas turbines. Consequently, these studies have shown that ammonia has the potential to replace hydrocarbon-based fuel, as mentioned previously [1]. In an effort to overcome the challenges associated with ammonia combustion, such as higher  $\text{NO}_x$  production, long ignition delay times, and lower laminar burning velocity (LBV), many researchers have started studying the effects of blending light and heavy fuels with ammonia to enhance combustion characteristics. Additionally, the buoyancy effect, a drawback in ammonia combustion, can be mitigated by increasing oxygen content, raising the initial temperature, or blending ammonia with fuels that have higher LBV. This section demonstrates the effect of fuel blending with ammonia on LBV, highlighting its potential for successful applications of ammonia as a fuel in various contexts.

Several fundamental studies on LBV enhancement of ammonia, blended with methane [19–26] and hydrogen [26–34], have been conducted both experimentally and numerically with additional hydrogen–methane blending [35–43] to optimize the accurate model prediction of oxidation models. The literature studies continuously show that a small fraction of  $\text{H}_2$  blended with  $\text{NH}_3$  or  $\text{CH}_4$  will increase the flame speed, despite the equivalence ratio and initial conditions. When 4%  $\text{NH}_3$  was blended with a  $\text{CH}_4$ -air mixture, Henshaw et al. [23] found that the LBV decreased by 17–23% as the mixture progressed from the lean to the rich side. Okafor et al. [21] reported a non-linear decrease in the LBV of the  $\text{CH}_4$   $\text{NH}_3$  flames with the  $\text{NH}_3$  addition (0–50%) and developed a kinetic model for  $\text{CH}_4$ - $\text{NH}_3$  flames. Moreover, they found that stretched LBV decreased as the mixture pressure and  $\text{NH}_3$  concentration increased, and the production of OH radicals in  $\text{CH}_4$ / $\text{NH}_3$ /air flames resulted in the formation of  $\text{NH}_2$  molecules, which greatly increased  $\text{NO}_x$  emissions; this blending improves the combustion characteristics of ammonia mixtures and reduces the  $\text{CO}_2$  emission as a result of low-carbon fuels with flame speeds higher than that of ammonia [20].

The blending of hydrogen is a logical attempt to achieve carbon-free flame and LBV enhancement instantly, thereby enhancing the flame. In the case of  $\text{H}_2$ / $\text{NH}_3$ , hydrogen exhibits higher mass diffusivity compared to ammonia. This makes hydrogen a promising additive for improving performance while minimizing  $\text{NO}_x$  and  $\text{N}_2\text{O}$  emissions in fuel-rich ammonia/air flames. Additionally, an increase in the blend of  $\text{H}_2$  tends to make the flame more sensitive to stretch. According to Lee et al. [44], the addition of 30–50%  $\text{H}_2$  blended with  $\text{NH}_3$  exponentially increased the LBV to 84%, thanks to the diffusivity and high

reactivity of hydrogen. As a result, the LBV reached a similar order of magnitude as that of a  $\text{CH}_4/\text{air}$  flame at approximately  $X_{\text{H}_2} = 40$

This study examines the use of hydrogen and methane as additives in ammonia-based combustion. It also explores the blending of ammonia with a single fuel. The structure of this study is as follows: Section 1 provides an introduction to the study and includes a literature review on ammonia blending. Section 2 describes the experimental setup, procedure, and data analysis method. Section 3 explains the kinetic models employed in the study. Section 4 presents the experimental results of combustion for ternary blend mixtures. Finally, Section 5 summarizes the future perspectives of ammonia-based combustion and concludes the study.

## 2. Experimental Setup and Methodology

Experiments were conducted in a high-pressure constant volume combustion chamber (CVCC) at the Mechanical Engineering Department of the University of Babylon, Iraq. A controllable injection system was manually and automatically controlled based on pre-calculated partial pressure data. The experimental setup is depicted in Figure 1, where direct measurements of the laminar flame speed were obtained for different fuel blending ratios. The chamber had an inner diameter of 305 mm, a length of 400 mm, and a thickness of 10 mm. Its volume was approximately 29 L. The mixture was ignited centrally using two spark electrodes with a diameter of 1 mm and a spark gap of 1.5 mm. An electronic circuit was employed to control the timing and power delivery, ensuring a strong spark. Two optical quartz windows, 120 mm in diameter and 20 mm thick, were positioned opposite each other to allow for monitoring and recording of flame propagation. A schlieren technique was utilized, using two lenses of plano-convex type with a high-speed camera (AOS-QPRI-Switzerland) with  $800 \times 800$  pixels. A controllable light source was used to visualize the flame.

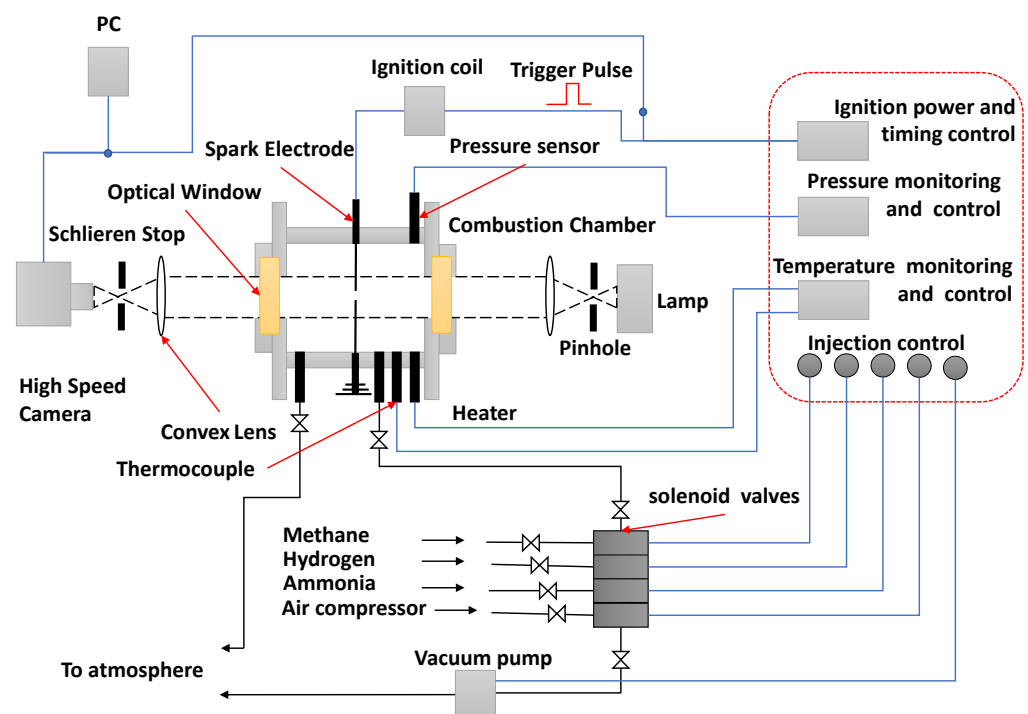


Figure 1. Schematic of the experimental setup.

Methane and ammonia were used as the main blending fuels; hence, this mixture blends with hydrogen, and the air was used as the oxidizer. A four-way manifold containing four solenoid valves was used to control the process of the mixture preparation; gaseous fuels, air injection, and exhaust gas scavenging. An electrical control board was utilized to

facilitate and regulate the experiments accurately by controlling the solenoid valves and regulating, controlling, and measuring the voltage entering the transformer. Furthermore, it was used to control and measure the initial pressure, temperature, and heating system.

In this study, the fuels can be blended according to two fractions of the fuel. Ammonia is the main fuel blended with methane based on the ammonia mole fraction ( $X_{NH_3}$ ) as shown in Equation (1). Moreover, hydrogen can be blended based on the hydrogen mole fraction ( $X_{H_2}$ ), computed as shown in Equation (2).

$$X_{NH_3} = \frac{V_{NH_3}}{(V_{CH_4} + V_{NH_3})} \tag{1}$$

$$X_{H_2} = \frac{V_{H_2}}{(V_{CH_4} + V_{NH_3} + V_{H_2})} \tag{2}$$

where  $V_x$  is the volume fraction of species  $x$  in the initial unburned fuel–air mixtures.

The experimental conditions for the mixing are summarized in Table 2. All experiments were conducted at an unburned mixture temperature of 298 K and variations in the temperature were kept within  $\pm 2$  K, which was monitored by a thermocouple; the initial mixture pressure of 0.1 MPa was measured and monitored by a pressure transmitter fixed on the combustion chamber. The main reasons for performing the experiments at an initial pressure of 0.1 MPa and an initial temperature of 298 K was to inhibit the development of Darrieus–Landau (DL), and due to the hydrodynamic instability of the finite flame thickness in relation to the flame size. The methane and ammonia blending ratio in this study varied from 100% to 0% with a 20% increment. The hydrogen additions to the main fuel were 0%, 20%, 40%, and 100%. The equivalence ratio was from 0.8 to 1.2, which is calculated according to the following relation:

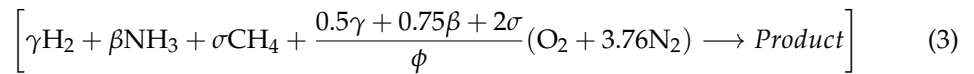


**Table 2.** Experimental conditions and H<sub>2</sub>/NH<sub>3</sub>/CH<sub>4</sub>/air flame parameters. The initial temperature was 298 K and  $\phi = 1$  \*.

Main Fuel %			H <sub>2</sub>	NH <sub>3</sub>	CH <sub>4</sub>	T <sub>prod</sub>	ρ <sub>u</sub> /ρ <sub>b</sub>	K <sub>R</sub> × 10 <sup>-2</sup>	C <sub>p,R</sub>	α <sub>R</sub> × 10 <sup>-5</sup>	ν <sub>R</sub> × 10 <sup>-5</sup>
H <sub>2</sub>	NH <sub>3</sub>	CH <sub>4</sub>	γ	β	σ	k		W/(m·k)	J/kg/K	m <sup>2</sup> /s	m <sup>2</sup> /s
0	0	100	0	0	1	2224	7.518	2.41	1077.9	1.59	1.98
	20	80	0	0.2	0.8	2210	7.507	2.41	1085.84	1.58	1.98
	40	60	0	0.4	0.6	2192	7.491	2.41	1096.21	1.58	1.97
	60	40	0	0.6	0.4	2167	7.467	2.41	1110.33	1.57	1.96
	80	20	0	0.8	0.2	2130	7.427	2.41	1130.72	1.57	1.95
	100	0	0	1	0	2072	7.350	2.41	1162.7	1.56	1.93
20	0	100	0.2	0	0.8	2234	7.471	2.60	1095.8	1.62	2.13
	20	80	0.2	0.16	0.64	2222	7.455	2.62	1105.46	1.621	2.15
	40	60	0.2	0.32	0.48	2208	7.435	2.64	1117.85	1.622	2.16
	60	40	0.2	0.48	0.32	2188	7.406	2.68	1134.35	1.625	2.18
	80	20	0.2	0.64	0.16	2160	7.363	2.72	1157.41	1.627	2.21
	100	0	0.2	0.8	0	2118	7.294	2.79	1191.91	1.63	2.25
40	0	100	0.4	0	0.6	2247	7.404	2.85	1121.48	1.66	2.35
	20	80	0.4	0.12	0.48	2239	7.384	2.89	1133.08	1.67	2.38
	40	60	0.4	0.24	0.36	2228	7.360	2.95	1147.62	1.68	2.42
	60	40	0.4	0.36	0.24	2214	7.328	3.01	1166.37	1.68	2.47
	80	20	0.4	0.48	0.12	2196	7.285	3.10	1191.49	1.70	2.53
	100	0	0.4	0.6	0	2170	7.223	3.22	1226.86	1.71	2.62
100	0	0	1	0	2378	6.875	4.95	1390.31	2.13	4.16	

\* dark gray for neat fuel, light grey for binary blending fuels, and white for ternary blending fuels.

To start each experiment, the initial step involves a vacuum process to purge the chamber of any residual gases. Following that, the flushing process is carried out to introduce fresh air into the chamber. Subsequently, a small amount of the blended fuel is introduced into the chamber from its storage tank, taking into consideration the partial

pressure (according to the Gibbs–Dalton law). This step is repeated for all three fuels. Finally, the chamber is injected with air. Afterward, the initial pressure and temperature are measured, all valves are closed, and camera settings, ignition power, and ignition timing are set. The mixture is now prepared for ignition. Data are recorded, and photographs are taken with a single trigger. The procedure of the experiment is mentioned in detail [45]. LBV was evaluated using the same procedure as in our previous study [14]. The stretched flame speed,  $S_N$ , was evaluated as follows

$$S_N = \frac{dr_{sch}}{dt} \quad (4)$$

where  $r_{sch}$  is the radius of the flame directly obtained from the schlieren photos and  $t$  is the progress time. The spherically propagating flame is influenced by the effects of flame stretch. In the present study, the flame stretch rate,  $\epsilon$ , was evaluated using the following linear equation

$$\epsilon = \frac{1}{A_F} \frac{dA_F}{dt} = \frac{2}{r_{sch}} \frac{dr_{sch}}{dt} = 2 \frac{S_N}{r} \quad (5)$$

where ( $A = 4\pi r_{sch}^2$ ) is the area of the flame front. Regarding the asymptotic analysis, an unstretched flame speed can be estimated using the nonlinear relationship in Equation (6).

$$\left(\frac{S_N}{S_S}\right)^2 \ln\left(\frac{S_N}{S_S}\right)^2 = -\frac{2L_b k}{S_S} \quad (6)$$

where  $L_b$  is the burned gas Markstein length. Thus,  $S_S$  can be calculated by the non-linear extrapolation of  $\epsilon \rightarrow 0$  (or  $r_{sch} \rightarrow \infty$ ).  $S_L$  can then be calculated by  $S_L = S_S \cdot \rho_b / \rho_u$

Here,  $\rho_b$  and  $\rho_u$  are the densities of the burnt gas and unburned mixture, respectively. Both densities were estimated from the thermal equilibrium, which was calculated by Chemkin-Pro.

Using a centrally ignited constant volume chamber to establish a spherical flame to estimate the unstretched LBV during a constant pressure period is well-known, but it introduces some uncertainties. These uncertainties include initial pressure fluctuation during filling, temperature fluctuations, radiation heat loss, buoyancy, ignition energy, and confinement. The accuracy of the pressure transducer, with an error of less than  $\pm 0.1$  KPa, is relatively small and can be ignored. Similarly, the confinement effect can be neglected since the outer diameter is larger (305 mm) than the optical window (120 mm), as required. The flame propagating profile can be divided into three regions: the ignition-affected region, the quasi-steady region, and the high-pressure and buoyancy-influenced regions. This study eliminates the effects of ignition energy and buoyancy by excluding the first and third regions and focusing on the quasi-steady regime.

Zheng Chen [46] investigated the accuracy of laminar flame speeds of methane fuel under standard temperature and pressure conditions (using multiple datasets from the literature). Uncertainties can arise from factors such as ignition energy, mixture preparation, buoyancy effect, cellular instability, confinement, radiation, nonlinear stretch behavior, and extrapolation methods. The study revealed that significant inconsistencies in laminar flame speed measurements were primarily attributed to uncertainties in achieving the proper equivalence ratio due to nonlinear stretch behavior and extrapolation. For lean, stoichiometric, and rich methane/air mixtures, the deviations in laminar flame speed measurements were approximately 40%, 8%, and 26%, respectively. Furthermore, it was observed that the discrepancies in the raw experimental data could be masked after extrapolation, affecting the results by 3–5% for lean mixtures. Nonlinear stretch behavior contributed up to 2% for lean mixtures, with a more pronounced effect at higher  $\phi$  (equivalence ratio). In this study, the total uncertainties, calculated using the approach employed by Dai et al. [47], were determined to range between 1.01 and 4.5 cm/s.

### 3. Kinetic Modeling Details

However, there are concerns arising from literature studies that highlight crucial inconsistencies between kinetic simulations and experimental results. These inconsistencies suggest that the prediction of laminar burning velocity (LBV) for ammonia–methane mixtures shows better agreement compared to ammonia–hydrogen mixtures, which requires further investigation. This indicates that there is no single model for ammonia oxidation capable of accurately predicting a wide range of ammonia blending with different fuels, emphasizing the need for comprehensive further research. Furthermore, the existing models cannot precisely cover a broad range of equivalence ratios and various initial pressures simultaneously. Lastly, the models fail to simultaneously predict both flame speed and  $\text{NO}_x$  emissions, with some models performing well in predicting NO formation but failing to accurately predict flame speed [27].

Li et al. [33] developed a reduced chemical model to estimate the combustion chemistry of hydrogen/ammonia/methane mixtures. Initially, the Aramco 2.0 model, Tian model, and Shrestha model were utilized to construct a detailed chemical model consisting of 128 species and 957 reactions. The compact reaction models were then derived through the directed relation graph with error propagation (DRGEP) method, combined with sensitivity analysis reduction. Ultimately, 2 reduced models were obtained: one comprising 51 species and 420 reactions, which included ammonia, hydrogen, and methane, and another with 28 species and 213 reactions, utilizing only hydrogen and ammonia. Both the detailed and reduced models exhibited good performance in terms of ignition delays, but they exhibited an over-prediction of laminar burning velocity (LBV) under fuel-rich conditions for both single ammonia fuel and mixtures.

Laminar flame speeds of ammonia with oxygen-enriched air and ammonia–hydrogen–air mixtures were experimentally studied by Shrestha et al. [31] using a constant volume combustion chamber. The experiments were conducted at a wide range of elevated initial pressures (1–10 bars) and elevated initial temperatures (298–473 K). The experimental data obtained from various setups, including freely propagating combustion chambers, burner-stabilized premixed flames, rapid compression machines (RCMs), shock tubes, and a jet-stirred reactor, were used to develop a newly validated kinetic prediction model for the oxidation of both neat ammonia fuel and ammonia–hydrogen-blended fuel. Increasing the initial temperature, hydrogen content in the fuel (ranging from 0 to 30% in volume), or the concentration of oxygen in the oxidizer resulted in an increase in the laminar flame speed. Conversely, increasing the initial pressure led to a decrease in the laminar flame speed. The suggested kinetic model accurately predicts the same trends as the experiments and demonstrates excellent agreement with the data across a wide range of conditions.

The LBV of premixed methane–ammonia–air mixtures was investigated both experimentally and numerically by Okafor et al. [20] across a wide range of equivalence ratios and ammonia concentrations. The ammonia concentration in the fuel varied from 0 to 30% in volume, represented as the heat fraction of ammonia in the fuel. The experiments were conducted in a constant volume chamber at a temperature of 298 K and a pressure of 0.1 MPa. As the concentration of ammonia increased, the laminar burning velocity exhibited a non-linear decrease. The experimental results were utilized to develop a detailed reaction model, employing the GRI Mech 3.0 [48] and the model constructed by Tian et al. [22].

Looking ahead, there is a crucial demand for a greater extent of supplementary experimental data on the LBV of ternary blending fuels to scrutinize the leftover uncertainties of ammonia oxidation.

This study examined the detailed models by Li et al. [33] (51 species), Okafor et al. [21], and Shrestha et al. [31], as shown in Table 3. The Chemkin-Pro 2021 R1 package [49] was utilized in this study to carry out all of the kinetic modelings that were included. Each investigated case used a minimum of 1000 grid points; the GRAD and CURV values were set to 0.02.

**Table 3.** Summary of the selected kinetic models.

Model	Species	Reactions	Fuels	Method	T (K)	P (MPa)	$\phi$
Li [33]	51	420	H <sub>2</sub> /NH <sub>3</sub> /CH <sub>4</sub>	Shock tube ignition delay modeling	1000–2000	0.1–5	0.5/1/1.2
Okafor [21]	59	356	NH <sub>3</sub> /CH <sub>4</sub>	Cylindrical constant volume chamber	298	0.1	0.8–1.3
Shrestha [31]	125	1099	H <sub>2</sub> /NH <sub>3</sub>	Spherical combustion chamber	298–473	0.1–1	0.7–1.7

### 4. Results and Discussions

#### 4.1. Laminar Burning Velocity of Single Fuel

The constant volume chamber method was validated by determining the LBV of the methane–air mixture and ammonia–air mixtures, as shown in Figure 2, at initial conditions of 298 K and 0.1 MPa, along with data from the preceding literature studies [19,26,33,41,50–52]. The concentration of ammonia was maximized on the richer side compared to methane, which is evident from the observed data. The current experimental data show consistency with published data, particularly in the stoichiometric region. Despite employing different methodologies to determine the laminar burning velocity (LBV), the current experimental data are well correlated with previous studies [26,30,51,53]. However, for pure ammonia, no experimental data were collected for lean ( $\phi = 0.8$ ) flames since it was difficult to collect data without increasing the ignition energy and, therefore, eliminating the bouncy effect, ensuring that the flames remained stable.

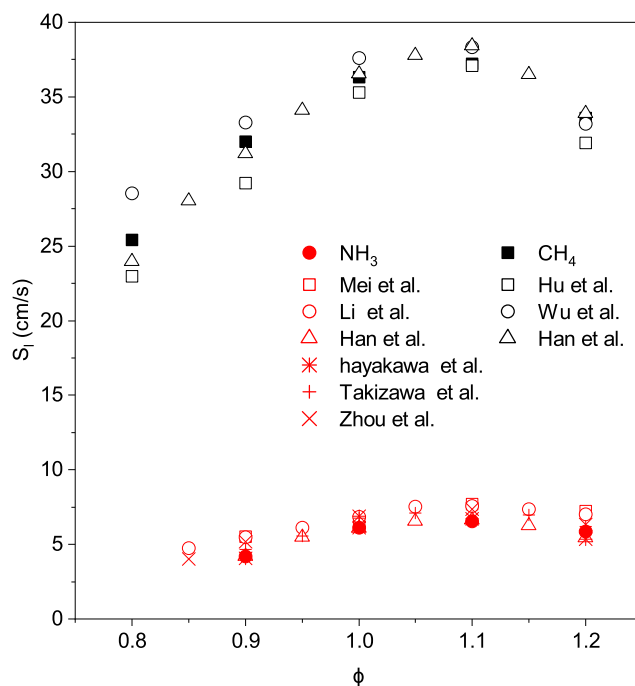


**Figure 2.** Summary of laminar burning velocity versus stoichiometric ratios for pure methane and ammonia fuels under atmospheric conditions, compared with those reported in the works of Hu et al. [41], Wu et al. [50], Han et al. [26], Mei et al. [52], Li et al. [54], Hayakawa et al. [51], Takizawa et al. [30], and Zhou et al [19].

#### 4.2. Laminar Burning Velocity of Binary Fuel Blending

In the previous Section 4.1, an illustration of the LBV for single-fuel air flames was validated experimentally; this subsection will present the binary fuel blends and the effect of ammonia blends.

**For NH<sub>3</sub>/H<sub>2</sub>/air flames,** the LBV is depicted in Figures 3 and 4B as a function of ammonia blend and equivalence ratios for 0%, 20%, and 40% hydrogen blends, respectively. The influence of hydrogen blending on the LBV exhibits a nonlinear dependency, as evidenced by this experiment, and the current experimental results demonstrate a higher

consistency with literature data [44,53]. Moreover, the figures show the predicted laminar burning velocities based on three different combustion models. All models underpredict the LBV, with the Li model [33] demonstrating the highest accuracy, and the Okafor model exhibiting the greatest underestimation. Shrestha’s model [31] considers  $\text{NH}_2 + \text{O} = \text{HNO} + \text{H}$ ,  $\text{NNH} + \text{O}_2 = \text{N}_2 + \text{HO}_2$  and  $\text{NH} + \text{OH} = \text{HNO} + \text{H}$  as very important reactions for predicting LBV, where the NNH radical is a key radical in the ammonia oxidation; the most important reactions are  $\text{NNH} + \text{O}_2 = \text{N}_2 + \text{HO}_2$ , where thermal dissociation competes with the oxidation reaction  $\text{NNH} = \text{N}_2 + \text{H}$ . Moreover,  $\text{N}_2\text{H}_2$  has a significant role, especially on the rich side [31]. It is worth noting that the equivalence ratio value at maximum LBV increases predominantly with hydrogen blending, going from 1.05 for pure ammonia to 1.10 for 40% hydrogen blends. The relationship between hydrogen blending and LBV exhibits a nonlinear dependency, as demonstrated by this experiment. This trend aligns with previous findings that the highest LBV for hydrogen–air flames occurs at  $\phi = 1.8$ .

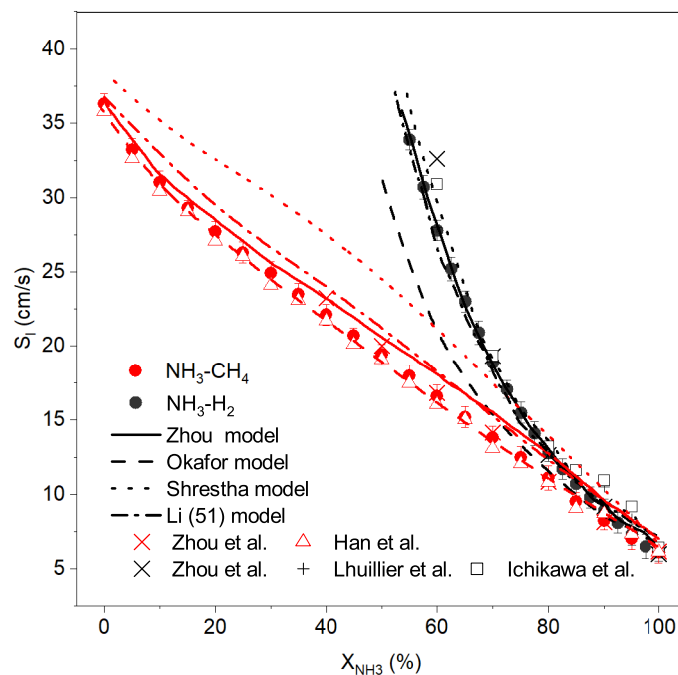


**Figure 3.** Summary of laminar burning velocity versus stoichiometric ratios for pure methane and ammonia fuels under atmospheric conditions, compared with those reported in the works of Zhou et al. [19], Han et al. [26], Lhuillier et al. [30], and Ichikawa et al. [28]

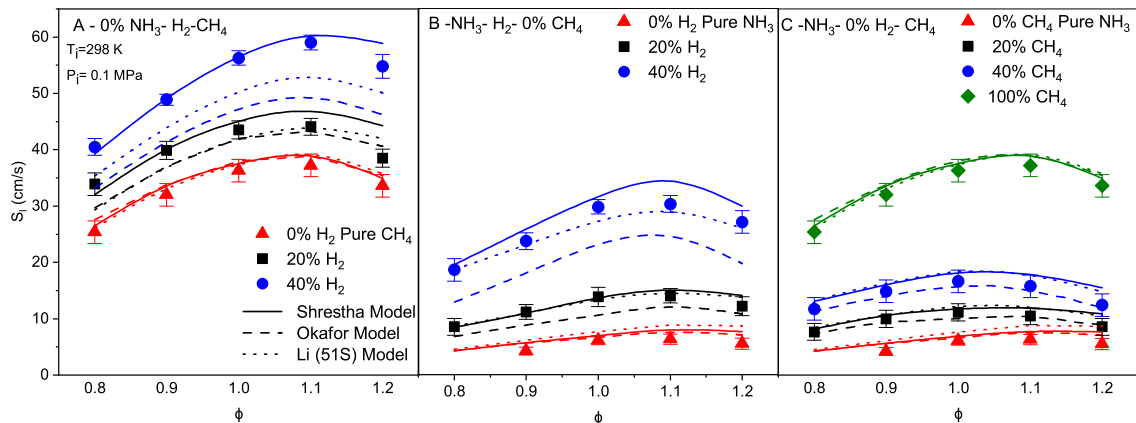


**Figure 4.** The LBV of dual fuel–air flames versus the equivalence ratio at 0.1 MPa and 298 K, for (A)  $\text{H}_2/\text{CH}_4$ ; (B)  $\text{NH}_3/\text{H}_2$ ; (C)  $\text{NH}_3/\text{CH}_4$  blends

It can be observed that none of the models are capable of accurately predicting the measured data. There are noticeable differences between the experimental and computed data, particularly on the rich side of the equivalence ratio. Furthermore, significant discrepancies exist among the computed results obtained from different models, especially with 40% hydrogen addition. It is important to note that these discrepancies between predictions and measurements become more pronounced as the equivalence ratio increases. The Okafor model significantly underpredicts the laminar burning velocity ( $SL$ ) in most initial conditions, indicating poorer performance compared to the parent model. The Shrestha model [31] accurately predicts  $SL$  on the lean side of stoichiometry, while it overpredicts it on the rich side. The Li model, however, demonstrates good predictions of  $S_L$  for all hydrogen blends.

For  $\text{NH}_3/\text{CH}_4/\text{air}$  flames, the laminar burning velocities of ammonia blended with methane at concentrations of 20%, 40%, 60%, and 80% are represented by the red color in Figures 3, 4C and 5A–D, respectively. These figures depict the laminar burning velocities as a function of equivalence ratios, where the ternary mixture contains 0% hydrogen fraction. The current experimental results demonstrate higher consistency with the literature data [19,26].

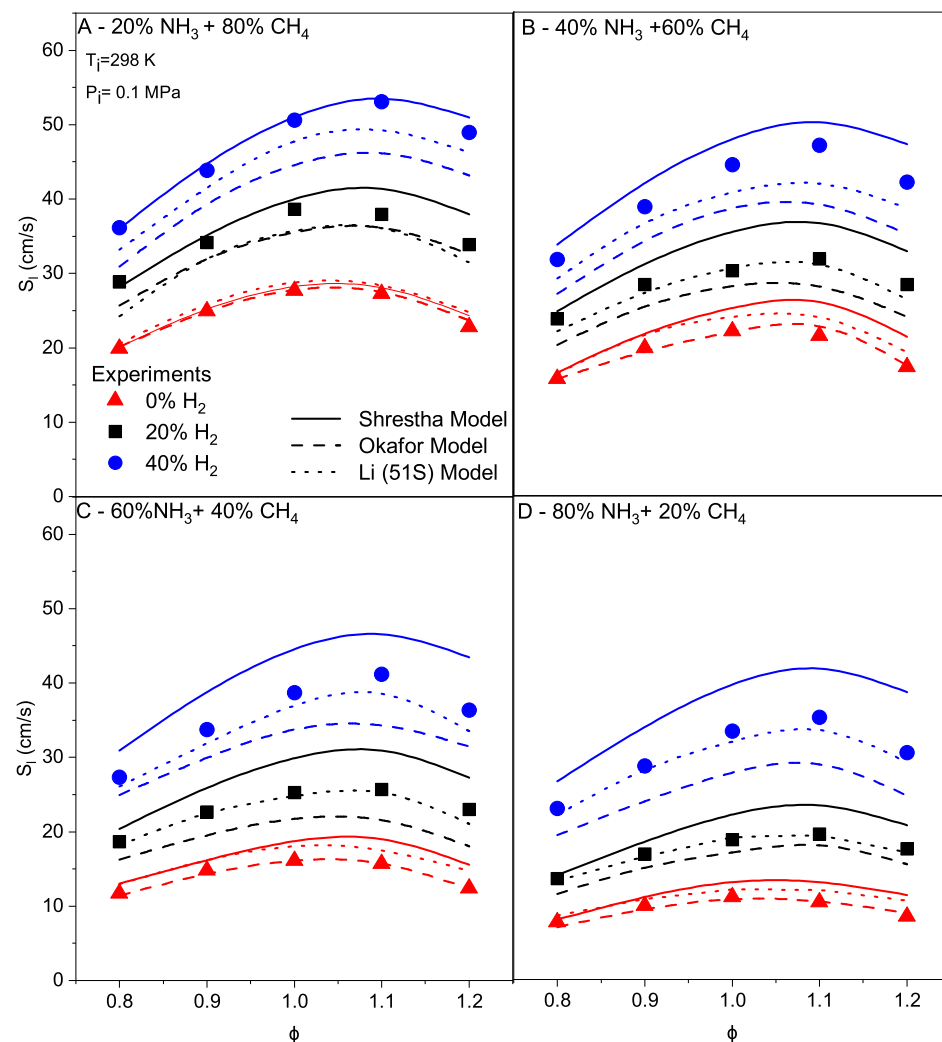


**Figure 5.** The LBV of ternary fuel–air flames are shown as percentages relative to different equivalence ratios at 0.1 MPa and 298 K. The fuel compositions for each case are as follows: (A) 20%  $\text{NH}_3$ /80%  $\text{CH}_4$ ; (B) 40%  $\text{NH}_3$ /60%  $\text{CH}_4$ ; (C) 60%  $\text{NH}_3$ /40%  $\text{CH}_4$ ; (D) 80%  $\text{NH}_3$ /20%  $\text{CH}_4$  for different  $\text{H}_2$  blends.

Furthermore, excellent consistency is shown between the experimental and predicted data from the Okafor [20] and Li [33] models, particularly in terms of predicting the laminar burning velocity ( $S_l$ ) values. Larger discrepancies can be observed for the Shrestha model data compared to the results of the other models, particularly on the rich side of the equivalence ratio. The Shrestha model shows good agreement with the experimental data in general for lean and stoichiometric conditions and higher ammonia fractions, while the Li model outperforms the Shrestha model on the rich side. Remarkable agreement, especially noticeable for  $\phi = 0.8$ , can be observed between the Okafor model and the experimental results. The three models demonstrate good performance throughout the range of the 20% ammonia blend, as methane already plays a dominant role in the combustion process. It is worth noting that the value of the equivalence ratio at which the maximum  $SL$  occurs remains constant at 1.05, regardless of the number of methane blends, for mixtures without any hydrogen blend. This behavior is clearly different from  $NH_3$  and  $H_2$  mixtures, as discussed previously.

The primary reason for the underestimation of the Li model [33] and Okafor model [20] is the dependency on the Tian model [22]. The  $HCO \rightarrow CO$  conversion pathway may be highly affected by the underestimation of LBV.  $HCO$  facilitates H radical production in the forward reaction  $HCO = CO + H$  and promotes the propagation of chain reactions, while  $HCO + H = CO + H_2$  atom transfer reactions have a chain-terminating character. In methane–ammonia flames, the reactions that take place between amine radicals and their products become more noticeable as the mixtures become richer, as does the impact on the burning [20].

**For  $H_2/CH_4$ /air flames**, the laminar burning velocities of methane with 0%, 20%, and 40% hydrogen blends are shown in Figure 4A. It can be observed that increasing the hydrogen blending leads to an increase in the LBV of the mixture, and the maximum  $S_l$  is shifted to the rich side of stoichiometry as the hydrogen blend increases. The predicted LBV for pure methane agrees well with the experimental data using different models. Regarding the hydrogen addition of 20%, the predicted data exhibit a similar trend, with an underestimation in the lean and stoichiometric regions and an over-prediction for the rich side. However, for the 40% hydrogen addition, significant discrepancies can be observed. The Li [33] and Okafor [20] models underpredict the LBV of all equivalence ratios, while the Shrestha model [31] demonstrates good agreement with the experimental results. The LBV grows non-linearly with increasing hydrogen concentration, and the discrepancies become more significant for mixtures with higher hydrogen concentrations.

#### 4.3. Laminar Burning Velocity of Ternary Fuel Blending

The LBV is the basic fundamental property of combustible mixtures and the key parameter in turbulent combustion. Based on the flame radius history in the large-scale combustion chamber, the  $S_l$  of  $NH_3/H_2/CH_4$  air mixtures are extracted using a non-linear approach.

Figure 6 illustrates the LBV of  $NH_3/H_2/CH_4$  air flames as a function of fuel blends at 0.1 MPa and 298 K. The left side of the figure displays the LBV of methane–hydrogen binary fuels, ranging from the 0 to 40% hydrogen fraction. It can be observed that the LBV increases non-linearly with the abscissa, showing a steeper slope for ammonia–hydrogen blends compared to ammonia–methane and methane–hydrogen blends. The minimum LBV value (for pure methane with  $X_{H_2} = 0$ ) corresponds to the maximum LBV value for  $NH_3/CH_4$  air flames (for pure methane with  $X_{NH_3} = 0$ ), and the LBV decreases non-linearly with increasing ammonia fraction. It is notable that the rapid increase in the LBV occurs after 20% hydrogen blending, when ammonia becomes the non-dominating fuel. Moreover, the impact of the 20% hydrogen addition in the ternary fuel is smaller compared to methane–ammonia flames. However, when the methane fraction exceeds 60% in the mixture with 20% hydrogen, a significant increase in LBV is observed.

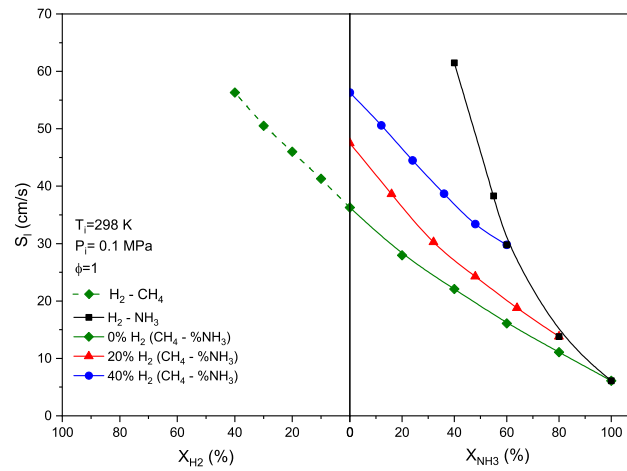


Figure 6. LBV of NH<sub>3</sub>/H<sub>2</sub>/CH<sub>4</sub> air flames versus fuel blends at 0.1 MPa and 298 K.

In order to compare the magnitude of enhancement on  $S_L$  due to the addition of H<sub>2</sub> and CH<sub>4</sub> to NH<sub>3</sub>/air flames, two normalized enhancement effect parameters are suggested, as follows:

$$\Gamma_{(\gamma,\beta,\sigma,\Phi),\%} = \frac{S_{l,M}(\gamma,\beta,\sigma,\Phi) - S_{l,NH_3}(\Phi)}{S_{l,NH_3}(\Phi)} \quad (7)$$

where  $S_{l,NH_3}(\Phi)$  is the LBV of the neat ammonia–air mixture that depends only on the equivalence ratio and  $S_{l,M}(\sigma,\beta,\gamma,\Phi)$  is the LBV of the ternary fuel–air mixture with  $M = (H_2(\gamma), CH_4(\sigma), \text{ and } NH_3(\beta))$ , as shown in Table 2, and that depends on blending ratios and the equivalence ratio. The enhancement parameter  $\Gamma$  is calculated using the present experimental data.

Figure 7 displays the enhancement parameter as a function of the hydrogen blending ratio, specifically at a ratio of 40%. It is evident that hydrogen has the highest impact on enhancing the LBV of ammonia/air flames, while methane has the lowest enhancement effect, regardless of the value of  $\phi$ . In the case of 40% hydrogen blending, the greatest enhancement impact is observed, with an increase of 820% compared to 550% for 0% hydrogen blending, both at  $\phi = 1$ . The degree of enhancement varies with blending ratios and  $\phi$ , with a more pronounced effect under fuel-lean conditions compared to rich fuel conditions.

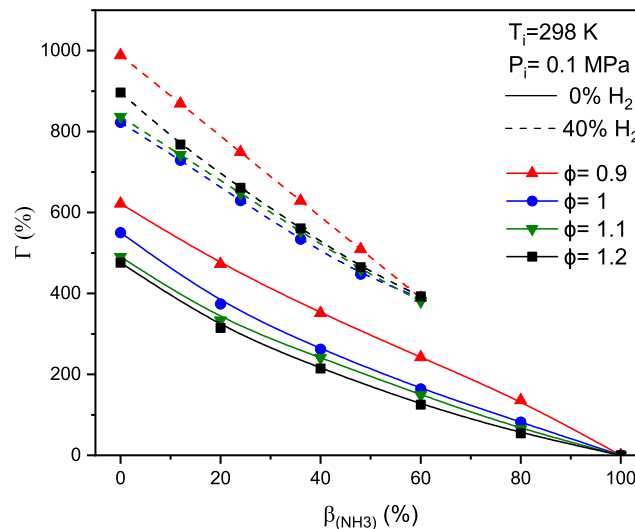


Figure 7. Enhancement effect on the LBV by adding 40% H<sub>2</sub> into NH<sub>3</sub>/CH<sub>4</sub>/air flames at  $\phi = 0.9–1.2$  at 0.1 MPa and 298 K.

Two important behaviors can be observed from the results. Firstly, when operating under the same stoichiometric ratio conditions, the enhancement achieved by using ternary fuels is much more favorable compared to using dual fuels. This impact remains consistent across the tests conducted in this study. For instance, to achieve an enhancement parameter  $\Gamma$  of 500% at  $\phi = 1$ , the dual fuel mixture requires 90% methane and 10% ammonia, while using ternary fuels allows for achieving the same  $\Gamma$  by blending 40% hydrogen with 36% ammonia and 34% methane. This mixture resolves the emission problem associated with a large blend of methane and also mitigates  $\text{NO}_x$  emissions with high ammonia blends. The second trend observed is that, as the hydrogen blending increases by 0%, 20%, and 40%, the enhancement parameter for the rich side of the stoichiometric condition also increases, surpassing the enhancement at stoichiometry for 40% hydrogen blending. This behavior arises because hydrogen becomes the dominant fuel in the mixture. These experimental values demonstrate the high potential of these fuel blends to enhance the LBV of ammonia/air flames when used in the appropriate blending ratios. This understanding is crucial for the future industrial application of ammonia combustion.

The other parameter is the normalized experimental LBV  $S_l^*$ , identified by the following equation:

$$S_{l(\gamma,\beta,\sigma,\Phi)}^* = \frac{S_{l,M}(\gamma, \beta, \sigma, \Phi)}{S_{l,CH_4}(\Phi)} \quad (8)$$

where  $S_{l,CH_4}(\Phi)$  is the LBV of the neat methane–air mixture that depends only on the equivalence ratio against the ammonia blending ratio for different hydrogen blends at an initial pressure of 0.1 MPa and initial temperature of 298 K. This parameter shows the blending effect related to the LBV of methane with respect to dual blending (ammonia and methane) and ternary blends (ammonia, hydrogen, and methane).

Figure 8 demonstrates the normalized LBV versus ammonia blends for 0, 20, and 40% hydrogen blends for a range of different equivalences ratios. The figure provides information on the influence of the ternary fuel effect that increases the LBV of 40% hydrogen starting from 75% to 160% of LBV of methane. For example, the influence of hydrogen addition to the ammonia–methane mixture on LBV can be achieved in the LBV of methane at an equivalence ratio of 1.2 by using 20% hydrogen, 64% methane, and 16% ammonia, or 40% hydrogen, 15% methane, and 45% ammonia. When the ammonia ratio is increased, there is a significant drop in the normalized velocity for zero hydrogen blends, especially for zero hydrogen blends. Nevertheless,  $S_l$  decreases only significantly with the increasing ammonia ratio. When the hydrogen ratio increases,  $S_l$  begins to grow noticeably for all equivalences ratios. It can be seen from the figure that the effect of hydrogen blending not only increases the laminar flame speed but also tends to the rich side to be maximized.

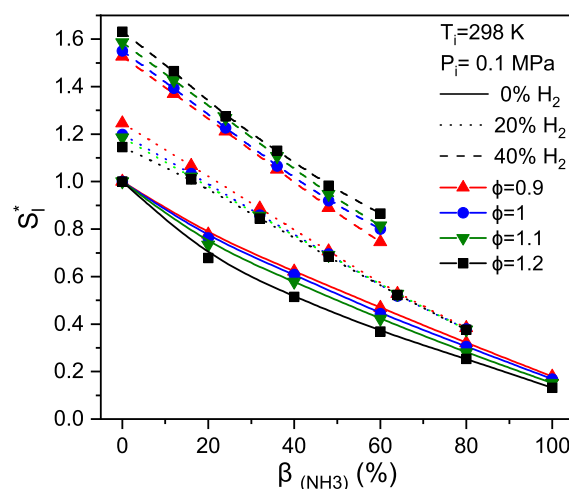


**Figure 8.** Normalized LBV of  $\text{NH}_3/\text{CH}_4/\text{air}$  flames versus  $\beta_{\text{NH}_3}$  of  $\sigma = 0, 20$ , and  $40\%$   $\text{H}_2$  blending at  $0.1$  MPa and  $298$  K.

To further demonstrate the effect of ternary fuel blending on the accuracy of the three models, laminar burning velocities are shown in black and blue in Figure 5A–D. Figure 5A shows the experimental data of laminar burning velocities based on 20% ammonia–80% methane–air flames with 0%, 20%, and 40% hydrogen blends compared with three different combustion models. One can see that the portion of ammonia will not affect the model's behavior. The Li [33] and Okafor [20] models underestimate any stoichiometric condition. In contrast, the Shrestha model [31] performs well for lean and stoichiometric conditions but tends to overestimate on the rich side due to an incomplete  $N_2H_i$  sub-mechanism and the doubling of the rate constant ( $NH_2 + NH = N_2H_2 + H$ ). The Li model [33] performed the best regarding the 60% ammonia–40% methane and 80% ammonia–20% methane–air flames with 20% and 40% hydrogen blends, as shown in Figure 5D,E. It seems that the Li model [33] is able to qualitatively predict the experimental trends of the lean and stoichiometric conditions when ammonia is the dominating fuel in the mixture.

Figure 9 shows the adiabatic flame temperature and density ratio for  $NH_3/CH_4$ /air flames as a function of  $\phi$  for both binary and ternary fuel blends. It can be observed that hydrogen yields the highest adiabatic flame temperature, while ammonia results in the lowest temperature. The effect of the tertiary fuel can be clearly seen in Figure 9B,D, distinguishing it from the dual fuel blends, which closely resemble the data for pure methane. The density ratio remains relatively constant on the lean mixture side for single, binary, and ternary fuels. The adiabatic flame temperature has a significant impact on the laminar burning velocity. Both the adiabatic flame temperature and density ratio reach their maximum values near stoichiometry and decrease for the lean and rich sides, which consequently affects the laminar burning velocity.

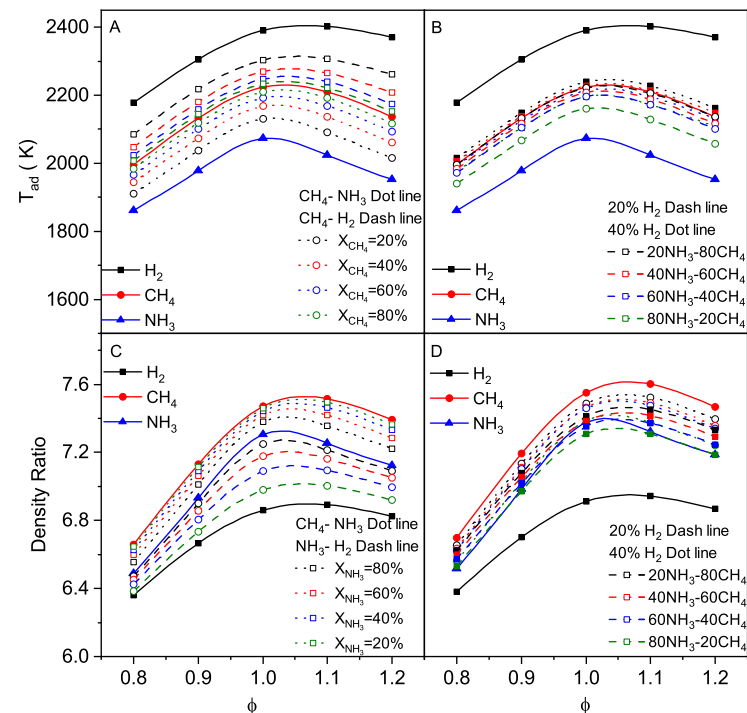


**Figure 9.** Adiabatic flame temperature of  $NH_3/CH_4$ /air flames versus  $\phi$  of (A) binary blending fuels; (B) ternary blending fuels; and density ratios for (C) binary fuels and (D) ternary fuels, at 0.1 MPa and 298 K.

## 5. Conclusions

This study investigates the flame propagation characteristics of ammonia/methane/air mixtures with molar ratios ranging from 0 to 100. A total of 20 were centrally ignited in an optically accessible constant volume combustion chamber at 0.1 MPa and 298 K. The effect of hydrogen blending from 0 to 40 on methane/ammonia blend fuels was examined.

Clarification is provided about the validity of various laminar combustion models for ammonia/methane/hydrogen–air flames. This study serves the following purposes:

- The LBV decreases non-linearly as the ammonia blending increases for both hydrogen and methane.
- When the hydrogen blend exceeds 20%, there is a noticeable increase in LBV for pure and dual fuel mixtures under all conditions.
- For methane flames with less than 50% ammonia fractions, the maximum LBV is on the slightly rich side of the equivalence ratio. Whenever the amount of methane or hydrogen in a mixture increases, the maximum LBV tends to move toward the rich side.
- The laminar burning velocities of ternary mixtures were estimated by comparing three models under constant temperature and pressure conditions. The Li model shows good agreement with experimental trends at lean and stoichiometric conditions, where ammonia is the dominant fuel in the mixture.
- The accuracy of the Li model appears to improve with an increase in ammonia concentration. Moreover, the Shrestha and Okafor models do not accurately predict the LBV of ternary mixtures. The validation of neat ammonia and methane demonstrates good agreement with prior findings in the literature, and the model predictions align well with experimental measurements.

## 6. Future Work

Investigations using different ternary fuel compositions are often insufficient for gaining comprehensive insights into the complexity of combustion. Additionally, it is crucial to study a broad range of hydrogen blending at different equivalence ratios in order to understand and quantify flame morphology. Similarly, exploring the pressure history of ternary fuel blends provides valuable information. Finally, the application of advanced deep learning algorithms can further enhance the investigation, optimization, and prediction of flame speed and other combustion characteristics, thereby facilitating the development of efficient fuel recovery processes.

**Author Contributions:** Conceptualization, J.W. and H.A.K.S.; methodology, A.Y., H.D. and A.A.A.A.; validation, A.Y., L.Z. and H.D.; resources, L.Z. and H.D.; Data curation A.Y., A.A.A.A. and L.Z.; funding acquisition, J.W. and Z.H.; writing—original draft, A.Y.; writing—review and editing, J.W. All authors have read and agreed to the published version of the manuscript.

**Funding:** This research was partially funded by the Major Science and Technology Projects of the Inner Mongolia Autonomous Region (2021ZD0021) and the Shaanxi Science and Technology Innovation Team (2021TD-22).

**Institutional Review Board Statement:** Not applicable.

**Data Availability Statement:** The data used in this study are reported in the paper's figures and tables.

**Conflicts of Interest:** The authors declare no conflict of interest.

## References

1. Kobayashi, H.; Hayakawa, A.; Somarathne, K.K.A.; Okafor, E.C. Science and technology of ammonia combustion. *Proc. Combust. Inst.* **2019**, *37*, 109–133. [[CrossRef](#)]
2. Law, C.K. *Combustion Physics*; Cambridge University Press: Cambridge, UK, 2010.
3. Hayakawa, A.; Goto, T.; Mimoto, R.; Kudo, T.; Kobayashi, H. NO formation/reduction mechanisms of ammonia/air premixed flames at various equivalence ratios and pressures. *Mech. Eng. J.* **2015**, *2*, 14-00402. [[CrossRef](#)]
4. Lewis, B.; Von Elbe, G. *Combustion, Flames and Explosions of Gases*; Elsevier: Amsterdam, The Netherlands, 2012.
5. Vandooren, J.; Bian, J.; Van Tiggelen, P. Comparison of experimental and calculated structures of an ammonia nitric oxide flame. Importance of the  $\text{NH}_2 + \text{NO}$  reaction. *Combust. Flame* **1994**, *98*, 402–410. [[CrossRef](#)]
6. Michalsky, R.; Parman, B.J.; Amanor-Boadu, V.; Pfromm, P.H. Solar thermochemical production of ammonia from water, air and sunlight: Thermodynamic and economic analyses. *Energy* **2012**, *42*, 251–260. [[CrossRef](#)]
7. Ritter, J.A.; Ebner, A.D.; Wang, J.; Zidan, R. Implementing a hydrogen economy. *Mater. Today* **2003**, *6*, 18–23. [[CrossRef](#)]

8. Okanishi, T.; Okura, K.; Srifa, A.; Muroyama, H.; Matsui, T.; Kishimoto, M.; Saito, M.; Iwai, H.; Yoshida, H.; Saito, M.; et al. Comparative Study of Ammonia-fueled Solid Oxide Fuel Cell Systems. *Fuel Cells* **2017**, *17*, 383–390. [[CrossRef](#)]
9. Miyazaki, K.; Okanishi, T.; Muroyama, H.; Matsui, T.; Eguchi, K. Development of Ni–Ba (Zr, Y) O<sub>3</sub> cermet anodes for direct ammonia-fueled solid oxide fuel cells. *J. Power Sources* **2017**, *365*, 148–154. [[CrossRef](#)]
10. Chiong, M.C.; Chong, C.T.; Ng, J.H.; Mashruk, S.; Chong, W.W.F.; Samiran, N.A.; Mong, G.R.; Valera-Medina, A. Advancements of combustion technologies in the ammonia-fuelled engines. *Energy Convers. Manag.* **2021**, *244*, 114460. [[CrossRef](#)]
11. Rocha, R.C.; Costa, M.; Bai, X.S. Combustion and emission characteristics of ammonia under conditions relevant to modern gas turbines. *Combust. Sci. Technol.* **2021**, *193*, 2514–2533. [[CrossRef](#)]
12. Kurien, C.; Mittal, M. Review on the production and utilization of green ammonia as an alternate fuel in dual-fuel compression ignition engines. *Energy Convers. Manag.* **2022**, *251*, 114990. [[CrossRef](#)]
13. Boretti, A. Novel dual fuel diesel-ammonia combustion system in advanced TDI engines. *Int. J. Hydrogen Energy* **2017**, *42*, 7071–7076. [[CrossRef](#)]
14. Yasiry, A.S.; Shahad, H.A. An experimental study of the effect of hydrogen blending on burning velocity of LPG at elevated pressure. *Int. J. Hydrogen Energy* **2016**, *41*, 19269–19277. [[CrossRef](#)]
15. Cai, X.; Wang, J.; Zhang, W.; Xie, Y.; Zhang, M.; Huang, Z. Effects of oxygen enrichment on laminar burning velocities and Markstein lengths of CH<sub>4</sub>/O<sub>2</sub>/N<sub>2</sub> flames at elevated pressures. *Fuel* **2016**, *184*, 466–473. [[CrossRef](#)]
16. Han, J.W.; Lee, C.E.; Kum, S.M.; Hwang, Y.S. Study on the Improvement of Chemical Reaction Mechanism of Methane Based on the Laminar Burning Velocities in OEC. *Energy Fuels* **2007**, *21*, 3202–3207. [[CrossRef](#)]
17. Hu, E.; Li, X.; Meng, X.; Chen, Y.; Cheng, Y.; Xie, Y.; Huang, Z. Laminar flame speeds and ignition delay times of methane–air mixtures at elevated temperatures and pressures. *Fuel* **2015**, *158*, 1–10. [[CrossRef](#)]
18. Chai, W.S.; Bao, Y.; Jin, P.; Tang, G.; Zhou, L. A review on ammonia, ammonia–hydrogen and ammonia–methane fuels. *Renew. Sustain. Energy Rev.* **2021**, *147*, 111254. [[CrossRef](#)]
19. Zhou, S.; Cui, B.; Yang, W.; Tan, H.; Wang, J.; Dai, H.; Li, L.; ur Rahman, Z.; Wang, X.; Deng, S.; et al. An experimental and kinetic modeling study on NH<sub>3</sub>/air, NH<sub>3</sub>/H<sub>2</sub>/air, NH<sub>3</sub>/CO/air, and NH<sub>3</sub>/CH<sub>4</sub>/air premixed laminar flames at elevated temperature. *Combust. Flame* **2023**, *248*, 112536. [[CrossRef](#)]
20. Okafor, E.C.; Naito, Y.; Colson, S.; Ichikawa, A.; Kudo, T.; Hayakawa, A.; Kobayashi, H. Experimental and numerical study of the laminar burning velocity of CH<sub>4</sub>–NH<sub>3</sub>–air premixed flames. *Combust. Flame* **2018**, *187*, 185–198. [[CrossRef](#)]
21. Okafor, E.C.; Naito, Y.; Colson, S.; Ichikawa, A.; Kudo, T.; Hayakawa, A.; Kobayashi, H. Measurement and modeling of the laminar burning velocity of methane–ammonia–air flames at high pressures using a reduced reaction mechanism. *Combust. Flame* **2019**, *204*, 162–175. [[CrossRef](#)]
22. Tian, Z.; Li, Y.; Zhang, L.; Glarborg, P.; Qi, F. An experimental and kinetic modeling study of premixed NH<sub>3</sub>/CH<sub>4</sub>/O<sub>2</sub>/Ar flames at low pressure. *Combust. Flame* **2009**, *156*, 1413–1426. [[CrossRef](#)]
23. Henshaw, P.F.; D’Andrea, T.; Mann, K.R.; Ting, D.S.K. Premixed ammonia–methane–air combustion. *Combust. Sci. Technol.* **2005**, *177*, 2151–2170. [[CrossRef](#)]
24. Arunthanayothin, S.; Stagni, A.; Song, Y.; Herbinet, O.; Faravelli, T.; Battin-Leclerc, F. Ammonia–methane interaction in jet-stirred and flow reactors: An experimental and kinetic modeling study. *Proc. Combust. Inst.* **2021**, *38*, 345–353. [[CrossRef](#)]
25. Shu, T.; Xue, Y.; Zhou, Z.; Ren, Z. An experimental study of laminar ammonia/methane/air premixed flames using expanding spherical flames. *Fuel* **2021**, *290*, 120003. [[CrossRef](#)]
26. Han, X.; Wang, Z.; Costa, M.; Sun, Z.; He, Y.; Cen, K. Experimental and kinetic modeling study of laminar burning velocities of NH<sub>3</sub>/air, NH<sub>3</sub>/H<sub>2</sub>/air, NH<sub>3</sub>/CO/air and NH<sub>3</sub>/CH<sub>4</sub>/air premixed flames. *Combust. Flame* **2019**, *206*, 214–226. [[CrossRef](#)]
27. Wang, S.; Wang, Z.; Elbaz, A.M.; Han, X.; He, Y.; Costa, M.; Konnov, A.A.; Roberts, W.L. Experimental study and kinetic analysis of the laminar burning velocity of NH<sub>3</sub>/syngas/air, NH<sub>3</sub>/CO/air and NH<sub>3</sub>/H<sub>2</sub>/air premixed flames at elevated pressures. *Combust. Flame* **2020**, *221*. [[CrossRef](#)]
28. Ichikawa, A.; Hayakawa, A.; Kitagawa, Y.; Somarathne, K.K.A.; Kudo, T.; Kobayashi, H. Laminar burning velocity and Markstein length of ammonia/hydrogen/air premixed flames at elevated pressures. *Int. J. Hydrogen Energy* **2015**, *40*, 9570–9578. [[CrossRef](#)]
29. Wang, N.; Huang, S.; Zhang, Z.; Li, T.; Yi, P.; Wu, D.; Chen, G. Laminar burning characteristics of ammonia/hydrogen/air mixtures with laser ignition. *Int. J. Hydrogen Energy* **2021**, *46*, 31879–31893. [[CrossRef](#)]
30. Lhuillier, C.; Brequigny, P.; Lamoureux, N.; Contino, F.; Mounaïm-Rousselle, C. Experimental investigation on laminar burning velocities of ammonia/hydrogen/air mixtures at elevated temperatures. *Fuel* **2020**, *263*, 116653. [[CrossRef](#)]
31. Shrestha, K.P.; Lhuillier, C.; Barbosa, A.A.; Brequigny, P.; Contino, F.; Mounaïm-Rousselle, C.; Seidel, L.; Mauss, F. An experimental and modeling study of ammonia with enriched oxygen content and ammonia/hydrogen laminar flame speed at elevated pressure and temperature. *Proc. Combust. Inst.* **2021**, *38*, 2163–2174. [[CrossRef](#)]
32. Goldmann, A.; Dinkelacker, F. Approximation of laminar flame characteristics on premixed ammonia/hydrogen/nitrogen/air mixtures at elevated temperatures and pressures. *Fuel* **2018**, *224*, 366–378. [[CrossRef](#)]
33. Li, R.; Konnov, A.A.; He, G.; Qin, F.; Zhang, D. Chemical mechanism development and reduction for combustion of NH<sub>3</sub>/H<sub>2</sub>/CH<sub>4</sub> mixtures. *Fuel* **2019**, *257*, 116059. [[CrossRef](#)]
34. Kumar, P.; Meyer, T.R. Experimental and modeling study of chemical-kinetics mechanisms for H<sub>2</sub>–NH<sub>3</sub>–air mixtures in laminar premixed jet flames. *Fuel* **2013**, *108*, 166–176. [[CrossRef](#)]

35. Mitu, M.; Razus, D.; Schroeder, V. Laminar Burning Velocities of Hydrogen-Blended Methane–Air and Natural Gas–Air Mixtures, Calculated from the Early Stage of  $p(t)$  Records in a Spherical Vessel. *Energies* **2021**, *14*, 7556. [CrossRef]
36. Salzano, E.; Pio, G.; Ricca, A.; Palma, V. The effect of a hydrogen addition to the premixed flame structure of light alkanes. *Fuel* **2018**, *234*, 1064–1070. [CrossRef]
37. Nilsson, E.J.; van Sprang, A.; Larfeldt, J.; Konnov, A.A. The comparative and combined effects of hydrogen addition on the laminar burning velocities of methane and its blends with ethane and propane. *Fuel* **2017**, *189*, 369–376. [CrossRef]
38. Huang, Z.; Zhang, Y.; Zeng, K.; Liu, B.; Wang, Q.; Jiang, D. Measurements of laminar burning velocities for natural gas–hydrogen–air mixtures. *Combust. Flame* **2006**, *146*, 302–311. [CrossRef]
39. Hermanns, R.; Konnov, A.; Bastiaans, R.; De Goey, L.; Lucka, K.; Köhne, H. Effects of temperature and composition on the laminar burning velocity of  $\text{CH}_4 + \text{H}_2 + \text{O}_2 + \text{N}_2$  flames. *Fuel* **2010**, *89*, 114–121. [CrossRef]
40. Coppens, F.; De Ruyck, J.; Konnov, A.A. Effects of hydrogen enrichment on adiabatic burning velocity and NO formation in methane+ air flames. *Exp. Therm. Fluid Sci.* **2007**, *31*, 437–444. [CrossRef]
41. Hu, E.; Huang, Z.; He, J.; Jin, C.; Zheng, J. Experimental and numerical study on laminar burning characteristics of premixed methane–hydrogen–air flames. *Int. J. Hydrogen Energy* **2009**, *34*, 4876–4888. [CrossRef]
42. TANOUE, K.; GOTO, S.; SHIMADA, F.; HAMATAKE, T. Effects of Hydrogen Addition on Stretched Premixed Laminar Methane Flames : 2nd Report, Effects on Flame Structure and Combustion Mechanisms. *Trans. Jpn. Soc. Mech. Eng. Ser. B* **2003**, *69*, 169–176. [CrossRef]
43. Okafor, E.C.; Nagano, Y.; Kitagawa, T. Experimental and theoretical analysis of cellular instability in lean  $\text{H}_2$ - $\text{CH}_4$ -air flames at elevated pressures. *Int. J. Hydrogen Energy* **2016**, *41*, 6581–6592. [CrossRef]
44. Lee, J.; Kim, J.; Park, J.; Kwon, O. Studies on properties of laminar premixed hydrogen-added ammonia/air flames for hydrogen production. *Int. J. Hydrogen Energy* **2010**, *35*, 1054–1064. [CrossRef]
45. Saleh, A.M.; Shahad, H.A.; Abdulraheem, A.A. Effect of Propane-Methanol Blending Ratio on the Stretched and Unstretched Flame Speeds at Elevated Initial Temperatures. *FME Trans.* **2022**, *50*, 121–130. [CrossRef]
46. Chen, Z. On the accuracy of laminar flame speeds measured from outwardly propagating spherical flames: Methane/air at normal temperature and pressure. *Combust. Flame* **2015**, *162*, 2442–2453. [CrossRef]
47. Dai, H.; Wang, J.; Cai, X.; Su, S.; Zhao, H.; Huang, Z. Measurement and scaling of turbulent burning velocity of ammonia/methane/air propagating spherical flames at elevated pressure. *Combust. Flame* **2022**, *242*, 112183. [CrossRef]
48. Smith, G.P. GRI-Mech Homepage. 1999. Available online: <http://www.me.berkeley.edu/gri-mech/> (accessed on 13 November 2022).
49. Design, R. CHEMKIN-PRO 15112. *San Diego* **2011**, *6*, 17–55.
50. Wu, Y.; Modica, V.; Rossow, B.; Grisch, F. Effects of pressure and preheating temperature on the laminar flame speed of methane/air and acetone/air mixtures. *Fuel* **2016**, *185*, 577–588. [CrossRef]
51. Hayakawa, A.; Goto, T.; Mimoto, R.; Arakawa, Y.; Kudo, T.; Kobayashi, H. Laminar burning velocity and Markstein length of ammonia/air premixed flames at various pressures. *Fuel* **2015**, *159*, 98–106. [CrossRef]
52. Mei, B.; Zhang, X.; Ma, S.; Cui, M.; Guo, H.; Cao, Z.; Li, Y. Experimental and kinetic modeling investigation on the laminar flame propagation of ammonia under oxygen enrichment and elevated pressure conditions. *Combust. Flame* **2019**, *210*, 236–246. [CrossRef]
53. Li, J.; Huang, H.; Kobayashi, N.; He, Z.; Nagai, Y. Study on using hydrogen and ammonia as fuels: Combustion characteristics and NOx formation. *Int. J. Energy Res.* **2014**, *38*, 1214–1223. [CrossRef]
54. Li, J.; Huang, H.; Kobayashi, N.; Wang, C.; Yuan, H. Numerical study on laminar burning velocity and ignition delay time of ammonia flame with hydrogen addition. *Energy* **2017**, *126*, 796–809. [CrossRef]

**Disclaimer/Publisher's Note:** The statements, opinions and data contained in all publications are solely those of the individual author(s) and contributor(s) and not of MDPI and/or the editor(s). MDPI and/or the editor(s) disclaim responsibility for any injury to people or property resulting from any ideas, methods, instructions or products referred to in the content.